Feed-Forward Neural Network for health monitoring of a parallel hybrid electric power system

Feed-Forward Neural Network for health monitoring of a parallel hybrid electric power system

M G De Giorgi[1,2], T Donateo[1,3], A Ficarella[1,4], N Menga[1,5], L Spada Chiodo[1,6] and L Strafella[1,7].

[1] University of Salento. Department of Engineering for Innovation, Lecce, 73100 Italy

[2]mariagrazia.degiorgi@unisalento.it
[3]teresa.donateo@unisalento.it
[4]antonio.ficarella@unisalento.it
[5]nicola.menga@unisalento.it
[6]ludovica.spadachiodo@unisalento.it
[7]luciano.strafella@unisalento.it

Abstract. Hybrid engines are becoming more and more widespread. Electric energy instead is a valid help to reduce the environmental impact. In hybrid engines, the number of components is higher and this results in a decrease in reliability. With Engine Health Monitoring (EHM) we mean the set of techniques used to monitor the health status of a system based on the values assumed by some related parameters. Artificial Intelligence (AI) methods are widely used nowadays in this discipline. In this paper, an EHM approach was developed to monitor the health status of some components constituting an hybrid turboshaft. The dynamic model of the hybrid electric power system is described in an accompanying paper. Feed-Forward Neural Network (FFNN) is used as AI tool to built the just cited system. The engine modelled with Simulink, was used to perform a series of steady-state simulations implementing a degradation condition in some selected components. The degradation condition was simulated by changing the value of the Performance Parameters (PPs) related to each of the selected components. The results of the simulation were used to obtain a dataset useful to train the FFNN to predict the values of the same PPs in a degraded case.

1. Introduction

Environmental pollution is one of the most relevant problems of our times. Part of the research efforts today is focused on the use of greener substitutes to the fuels widespread [1] [2] [3]. Also the aeronautical industry is subject to the implications of the problem. Indeed, typical conventional thermal engines exploit the combustion process to obtain the chemical energy possessed by the fuels and this inevitably leads to emissions, contributing to global pollution [4] [5]. Nowadays technology points to the development of hybrid engines, which are constituted by both thermal and electric motors, to use both chemical and electric energy respectively as a source to produce thrust. The main concept is to exploit electric energy to produce a part of the thrust required during a flight mission, which leads to a lower level of pollutants compared with the classical chemical one. At the actual technology level, the power/weight and power/volume ratios of batteries is still not high enough to autonomously power an aircraft for medium/long distances. A hybrid engine is made of components typical of both thermal

engines and electric motors, such as a compressor, turbine, or burner (typical components of a thermal engine) and battery or dynamo (typical components of an electric motor). This increase in components number, however, leads to a decrease in the global hybrid engine reliability. Due to the key role assumed by reliability in the aeronautical sector, some interventions are necessary to face this problem. Nowadays, Engine Health Monitoring (EHM) discipline is very widespread as an approach to continuously monitoring the health status of an engine, developing a condition-based maintenance plan, which permits to avoid some inefficient situations, such as premature overhaul or in-flight engine failure, and intervention only when the engine is in a condition of advanced degradation [6] [7]. Degradation instead is a stochastic event that depends on many factors and which can affect engines in different ways and severities. Degradation can affect many engine components, such as compressor, turbines, burner, mechanical transmissions and also batteries, in the case of a hybrid engine. The most relevant degradation phenomena are compressor fouling and turbine erosion. Compressor fouling, which is the most relevant degradation phenomenon [8], is given by the accumulation of air contaminants, such as dust, dirt, sand on blades and walls. This results in a change of the air passage area, blade roughness and blade aerodynamic shape, which a decrease in efficiency and flow parameter [9]. Fouling can affect other engine components, however, being the compressor the first component in the gas-path (or fan, in turbofan engines), it is the most affected component by this phenomenon. Fouling is relevant in the first stages of compressors and some of the performance loss due to it can be recovered by washing. Turbine erosion instead, refers to a gradually loss of material from blades and walls due to impact with bigger air and combustion gases contaminants. This leads again to a change in the aerodynamic shape, roughness, and air passage area with a consequent decrease of turbine performance as the efficiency and an increase in flow parameter [10]. Degradation can also manifest itself in the electric portion of an hybrid engine in the battery. The battery a very important component for the electric section of an hybrid engine, being the one that stores electric engine. An older and degraded battery can deliver a lower power compared with a healthy one. Otherwise, also its autonomy decrease. Battery degradation is related to working temperature, discharging current rate, charging rate, depth of discharge, and time intervals between full charge cycles [11] [12]. The effects of sand and dust are investigated in [13]. In [13] two experiments are illustrated, characterized by two different sand ingestion rates. Results of both experiments show a decrease in thrust and an increase in specific fuel consumption. The effect of another air contaminant, i.e. volcanic ash, is investigated in [14]. The study focuses on the erosive effects of volcanic ash on fan blades, highlighting a higher erosion rate at the tips. In [15] there is a description of typical problems which can affect a battery located in a hybrid engine. Artificial Intelligence (AI) algorithms are widely used for EHM purposes. In [16] Artificial Neural Networks (ANNs) have been trained for performance prediction purposes, to predict Exhaust Gas Temperature (EGT) and fuel flow rate (w_f), and for engine fault prediction, considering three degradation cases, i.e. compressor fouling and turbine erosion considered individually and simultaneously. ANNs have been also used in [17] for performance prediction and fault classification, considering the same degradation cases mentioned in the previously cited paper. Results are compared with the one obtained from the application of Support Vector Machine (SVM). Better results have been obtained in performance prediction by ANNs, vice-versa SVMs show better behavior in fault classification. In [18] a two-steps tool has been developed, based on ANNs. The system predicts some measurable parameters based on flight data and in case of a high difference between measured and predicted values the second part of the tool is activated to detect which component is degraded. In [19] Levenberg-Marquardt Feed-Forward Neural Network (FFNN) and Radial Basis Function Network are exploited for EGT prediction, with better performance obtained by the first cited technique. In this paper, a FFNN is the AI tool used to develop the goal system. A virtual model of a turboshaft engine, develop with Simulink, has been used to perform a series of steady-state simulation in degraded condition. The results so obtained were used to train a FFNN to predict some Performance Parameters (PPs) used as health index of some engine components. The degradation condition considered is a scenario in which compressor, burner, shaft mechanical transmissions, electric motor and battery are all in a degraded state of different and casual level. For each steady-state

simulation the level of degradation of each component is different and randomly obtained. Degradation state was implemented in the engine model by changing the value of the PPs respect to the healthy case. The variables chosen as PPs are isentropic efficiency and flow parameter for compressor, pneumatic and combustion efficiency for burner, high and low-pressure shaft mechanical efficiencies for spools, efficiency for electric motor and internal resistance for battery.

2. The hybrid electric power system

The propulsion system considered in this investigation is designed for an application of Urban Air Mobility and consists of a coaxial rotor and a parallel Hybrid Electric Power System (HEPS). The rotor is connected to the turboshaft engine and a couple of identical electric motors which are fed by a Li-ion battery.

The HEPS is modeled with the flowchart of Figure 1 implemented in the Matlab/Simulink simulation environment. A Pilot Interpreter block translates the PLA command and the flight conditions (altitude and Mach) into a power request using a predefined map, obtained through comparison with an analogous engine available in GSP, which has been used as reference for the development of the present model. The power request is split between the engine and the motors by a predefined energy management strategy, that takes into account not only the power request but also the battery state of charge and state of health. This strategy, implemented by a supervisory controller, is based on fuzzy logic rules established in [20]: at any time-instant, the controller takes in input total power request, battery State of Health (SoH) and the deviation of the actual State of Charge (SoC) from a reference value which represents the optimal battery discharge curve along a given mission [21]. The output of such fuzzy logic determines the split of electric to total torque (henceforth named electric contribution k) and thus the torque set points for the thermal and electric machines. However, this step will be skipped in the present investigation since it deals with steady state operating points characterized by a user-defined power split, so a deeper analysis of the supervisory controller working principle is beyond the scope of this work. For major details, refer to [20], [21].

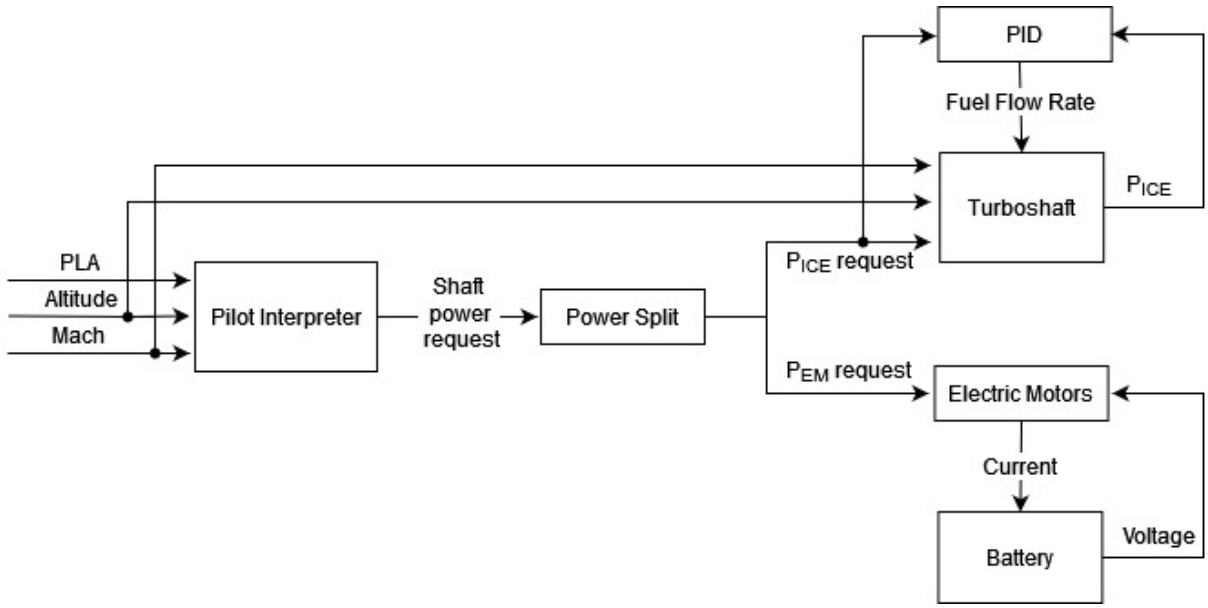

Figure 1. Flowchart of the Simulink model.

From the engine torque setpoint, the turboshaft model calculates the fuel flow rate and the other engine outputs by means of an in-house model implemented in Simulink and incorporating steady-state and dynamic parameters obtained from the GSP libraries [22].

The steady-state parameters include the maps of each turbomachinery (pressure ratio and isentropic efficiency vs corrected flow rate), the mechanical efficiency of the two shafts, the combustion and pneumatic efficiency of the burner. The dynamic parameters include the values of the inter-component volumes at the exit of the burner and of the High Pressure Turbine (HPT) that account for accumulation effects during transient phases. The pressure variations in these volumes are obtained by solving the following equation (1):

$$\frac{dp}{dt} = \frac{RT}{V}\frac{dm}{dt} = \frac{RT}{V}(\dot{m}_{in}\text{-}\dot{m}_{out}) \tag{1}$$

where p and T are pressure and temperature inside the volume, V is the volume of the plenum, R the specific gas constant and the parenthesis represents the accumulation inside the volume.

In the proposed two-spool engine the compressor and the High-Pressure Turbine are connected through the High-Pressure spool and the Low-Pressure Turbine delivers its power output to the rotor shaft. The Low-Pressure shaft is assumed to rotate at a constant speed (6000 rpm) because the rotor dynamic is not considered at this stage of the investigation.

A power balance is applied to the HP spool accordingly to equation (2):

$$\dot{N}_{gg} = \left(\frac{30}{\pi}\right)^2 \frac{1}{I \cdot N_{gg}} (P_{HPT} - P_C) \tag{2}$$

where the shaft acceleration $\dot{N}_{gg}$ is expressed as a function of power mismatch between HPT power output and compressor power request, shaft inertia I and current rotational speed N_{gg}. After model initialization, the engine attains a steady-state condition with the HPT power output balancing the compressor power request.

The fuel flow rate is determined by a PID controller (whose parameters have been adjusted with an automated tuning procedure) which acts on the LPT power output error, so that the delivered fuel allows the engine to match its power demand.
The scheme of the turboshaft is reported in Figure 2.

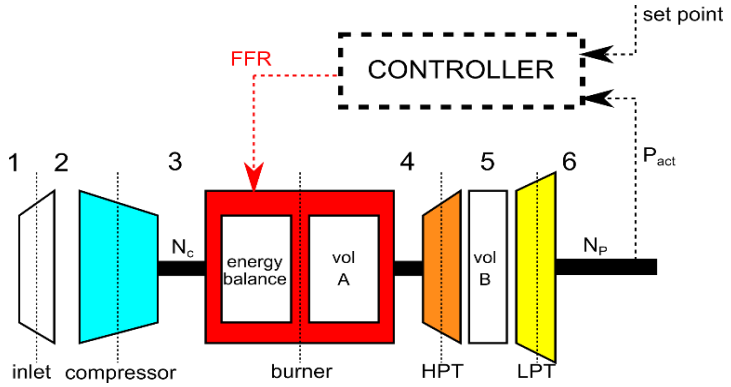

Figure 2. Scheme of the turboshaft engine.

The electric motors are modeled through Simulink Mapped Motor block, which maps torque-speed envelope and motor efficiencies over the operating range. It also includes a time constant for motor and drive response (Mapped Motor [23]).

The battery consists of 73 cells in series with a nominal voltage of 270V and a nominal capacity *C*. The battery is modeled with an equivalent circuit [24] with actual voltage *V(t)* given by:

$$V(t) = OCV - R_i \cdot I(t) \tag{3}$$

where OCV is the open circuit voltage, which depends on battery SoC and R_i is its internal resistance.

Peukert effect is accounted for by assigning a Peukert coefficient *n* to calculate battery effective current given battery nominal current I_{nom} (equation (4)); moreover, the effect of battery operating temperature is taken into account when evaluating battery actual capacity, as suggested in [25]. Consequently, the actual battery SoC is calculated as :

$$I_{eff}(t) = I(t) \cdot \left[\frac{I(t)}{I_{nom}}\right]^{n-1} \tag{4}$$

$$SoC(t) = SoC(t_0) - 100 \cdot \int_{t_0}^{t} \frac{I_{eff}(t)}{C} \left(\frac{T_{ref}}{T}\right)^{\beta} dt \tag{5}$$

In equation (5), T_{ref} is the reference operating temperature (namely 300 K) and β is the temperature coefficient obtained from [25]. Both R_i and *n* are battery performance parameters, whose degradation will be analyzed in this investigation together with the effect of battery working temperature.
The electric path is depicted in Figure 3.

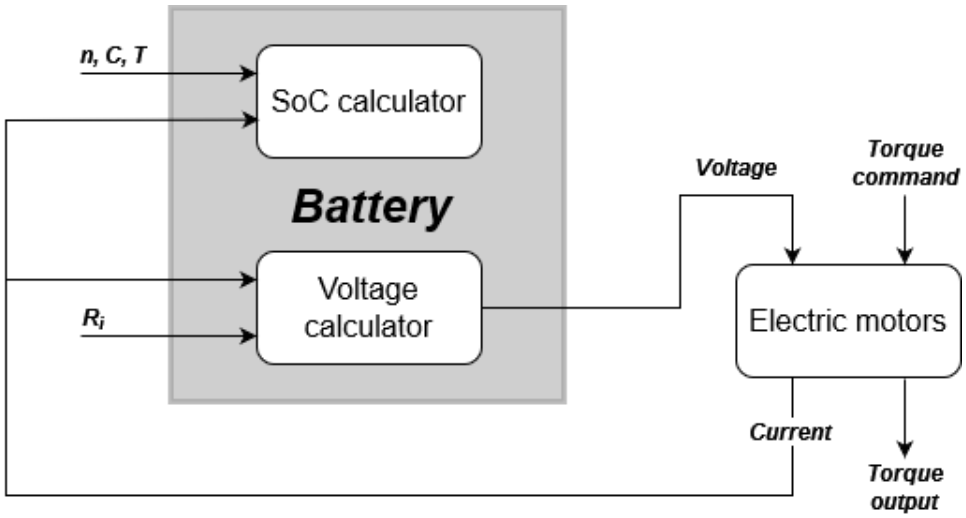

Figure 3. Battery and electric motors.

The whole model of the HEPS is explained in details in the accompanying paper “A dynamic model of a Hybrid Electric Propulsive System for degradation assessment”.

3. Simulated degradation condition

The tool aims to predict the value of some non-measurable parameters (the PPs) based on the value of some measurable ones. The measurable parameters can be flight data and state variables, obtainable

using adequate sensors. To do this, the FFNN must be trained on the correlation existing between the measurable variables (which are input variables for the neural network) and the PPs to be predicted (which are output variables for the neural network). Simulation results are very useful for this purpose. In this section, the details of the performed simulations are reported, in terms of degraded components, chosen PPs (i.e. output variables for the neural network), and variables selected as input one for the neural network.

In Table 1 the components chosen to be degraded are reported, together with the related PPs, their values in healthy conditions and the range of variation with respect to a healthy condition. The term "CF" stands for "corrective factor" and indicates that PP that accompanies it has been changed by applying a corrective factor and not by changing the parameter itself, therefore the relative data refer to the corrective factor and not to the PP.

Table 1. Degraded components, PPs (or their CFs), their value in healthy conditions and range of degradation level.

Component	Degraded performance parameters	Healthy condition	Range of percentage variation
Compressor	Isentropic efficiency (η_c) (CF)	1	0 ÷ -20%
	Corrected mass flow rate (f_c) (CF)	1	0 ÷ -20%
Burner	Pneumatic efficiency ($\eta_{b,p}$)	0.96	0 ÷ -20%
	Combustion efficiency ($\eta_{b,c}$)	0.985	0 ÷ -20%
Shaft transmissions	High-pressure shaft mechanical efficiency (η_{HPS})	0.99	0 ÷ -20%
	Low-pressure shaft mechanical efficiency (η_{LPS})	0.99	0 ÷ -20%
Electric motor	Efficiency ($\eta_{e,m}$) (CF)	1	0 ÷ -20%
Battery	Internal resistance (R_i) (CF)	1	0 ÷ +20%

As already mentioned, a series of steady-state simulations have been performed which correspond to some degradation conditions in each of the components reported in Table 1. In each simulation, the degradation level of each component was randomly obtained. Four different working conditions have been considered (taken from real missions, in turn, taken from [26]), which differ in flight speed (vf), altitude (h), required power, Power Lever Angle (PLA), battery state of charge and electric contribution (Ec) to the total required power. Table 2 reports the just cited working points.

Table 2. Simulated working points.

Working point name	Speed (m/s)	Altitude (m)	Required power (KW)	PLA (%)	Battery state of charge (%)	Electric contribution (%)
MAXPOW-A	30.6	0	289	65.3	97	40
MAXPOW-B	4	1154	267	68	99	47
MAXDUR-A	30.6	492	167	50.3	85	70
MAXDUR-B	0	2550	171	61.5	78	60

A total of 773 steady-state simulations have been performed, using the four working points reported in Table 2. The obtained results have been divided to build a training dataset (used to train the neural network to learn the input and the output variables) and a test dataset (used to test the performance of the previously trained network). The train dataset is constituted by 526 observations of a total 773. The test dataset is constituted by the remaining 247 observations. Table 3 describes the observations contained in train and test datasets.

Table 3. Train and test datasets observations.

	Training	Testing
MAXDUR-A	170 steady-state observations	80 steady-state observations
MAXDUR-B	167 steady-state observations	79 steady-state observations
MAXPOW-A	102 steady-state observations	48 steady-state observations
MAXPOW-B	87 steady-state observations	40 steady-state observations

As mentioned before, each simulation is characterized by a different degradation level for each component. The degraded values of the PPs used to implement the degradation were randomly obtained considering the degradation range reported in Table 1. The following equation was used to calculate the degraded values of the PPs:

$$pp_d = \left[1 - \left(1 - \frac{MIN}{MAX}\right) RAN^3\right] MAX \tag{6}$$

where pp_d is the degraded value of the PP, MIN and MAX are respectively the lower and the upper limits considered for the PP for which the equation is being used and RAN is a randomly generated number in the interval $0 \div 1$. To permit the FFNN to predict the goal variables (i.e. the PPs) it must be trained with some other variables physically correlated with them. This information can come from a series of sensors installed through the powertrain. The variable to be predicted are related to the performance of the degraded components, which in turn depend on the value of some other parameters related to the working condition at which the component work, such as inlet and outlet temperatures and pressures for thermal section, or current and voltage for an electric one. In neural network logic, the variable used to inform it are called input variables, while the variables to be predicted are called output variables. Table 4 and Table 5 show the input and the output variables respectively chosen in this work.

Table 4. Input variables for FFNN.

Input	
Power Lever Angle (PLA)	Total press. at burner outlet (TP_4)
Altitude (h)	Total temp. at HPT outlet (TT_5)
Flight speed (v_f)	Total press. at HPT outlet (TP_5)
Electric contribution (E_c)	Total temp. at LPT outlet (TT_6)
Battery delta temp. respect to clean status (ΔT)	Total press. at LPT outlet (TP_6)
Total temp. at compressor inlet (TT_2)	Compressor shaft speed (ω_{HPS})
Total press. at compressor inlet (TP_2)	Fuel mass flow rate (w_f)
Total temp. at compressor outlet (TT_3)	Overall pressure ratio (OPR)
Total press. at compressor outlet (TP_3)	Battery current (I)
Total temp. at burner outlet (TT_4)	Battery voltage (V)

Table 5. Output variables for FFNN.

Output
η_c (CF)
f_c (CF)
$\eta_{b,p}$
$\eta_{b,c}$
η_{HPS}
η_{LPS}
$\eta_{e,m}$ (CF)
R_i (CF)

4. Developed system: FFNN for performance prediction

In this section, a brief explanation of what an ANN is reported. Subsequently, there is a description of the system developed by using the FFNN type.

An ANN is an algorithm having the ability to emulate the behaviour of the human nervous system to learn from experience. The basic elements of an ANN are neurons. The neurons are organized in layers. The neurons of a layer are connected by a weighted connection to the neurons of the previous or next layer. A series of layers, constitute the ANN. ANN is constituted by an input layer (constituted by the so-called input neurons and in which information is entered in the ANN), an output layer (constituted by the so-called output neurons and from which the ANN prediction comes), and one or more hidden layers (constituted by the so-called hidden neurons), which are located between the input and the output layer. The prediction performance of the ANN depends on the number of hidden layers and hidden neurons. The information enters the ANN from the input layer and propagates through the hidden layers until it reaches the output layer. The neurons located in hidden and output layers combine the information deriving from the neurons located in the previous layers as described by equation (7):

$$z = \sum_{i=1}^{n} W_i I_i + b \tag{7}$$

where z represents the neuron output, W_i is the weight of the link between the neuron in question and the i-th neuron that sends it information, I_i is the information sent by the i-th neuron, n is the number of neurons that send information to the neuron in question and b is an added bias. Subsequently, an activation function is applied to normalize the result obtained from equation (7). In the training phase, the neural network is informed both with input variables and the related output variables and the algorithm calculates the value of the connection weights and biases to minimize the error between the prediction and the output variables. Figure 4, shows a typical structure of the FFNN used in this paper. As mentioned above, the network performance depends on the number of hidden neurons and layers. The optimal number can be obtained through a sensitivity analysis, to understand how performances vary as the above parameters vary. The FFNN used in the developed EHM system has only 1 hidden layer which activation function is the symmetric sigmoid transfer function, formed by 20 hidden neurons. The early stopping method has been used to improve generalization. Hence the available data is divided into three subsets. The first subset is the training set, which is used for computing the gradient and updating the network weights and biases. The second subset is the validation set. The error on the validation set is supervised during the training process. The validation error generally decreases during the initial phase of training. But, when the network begins to overfit the data, the error on the validation set typically starts to increase. If the validation error rises for a specified number of iterations, the training is stopped, and the weights and biases at the minimum of the validation error are returned.

Some error metrics have been used to have feedback about the prediction performance. The used metrics are:

- Mean Squared Error (MSE)
- Normalized Mean Squared Error (NMSE)
- Root Mean Squared Error (RMSE)
- Normalized Root Mean Squared Error (NRMSE)
- Mean Absolute Error (MAE)
- Mean Absolute Relative Error (MARE)
- Coefficient of Correlation (CoC)
- Coefficient of Determination (CoD)
- Coefficient of Efficiency (CoE)
- Maximum Absolute Error (MaxAE)

- Maximum Absolute Relative Error (MaxARE)

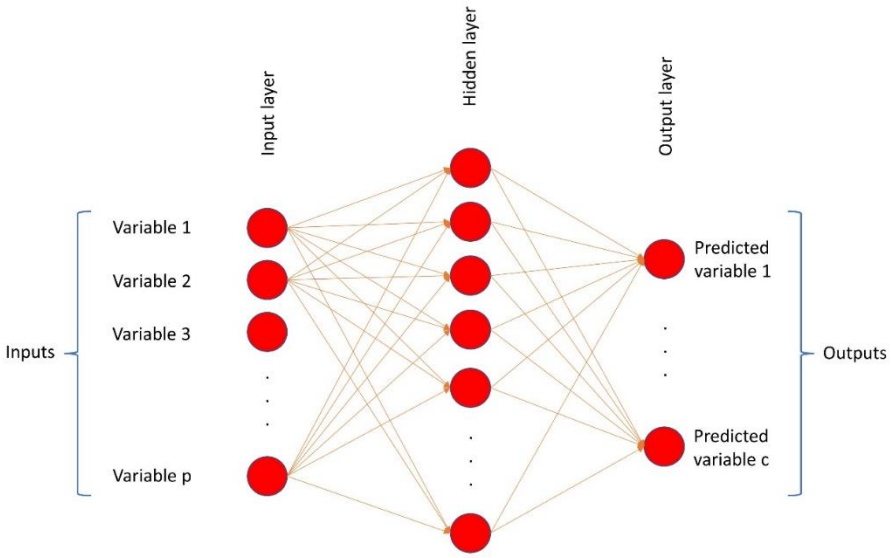

Figure 4. A typical FFNN structure.

The MSE is calculated with the following equation:

$$MSE = \frac{\sum_{i=1}^{s}(p_i - t_i)^2}{s} \tag{8}$$

where in our work p is the prediction, t is the target value and s is the number of observations. Since in a dataset the variables can have a different scale, a normalization process help to improve the comparison between them. NMSE and the other used metrics are defined by the following equations [27] [28]:

$$NMSE = \frac{\sum_{i=1}^{s}(E_i)^2}{s} \tag{9}$$

$$RMSE = \left(\frac{\sum_{i=1}^{s}(p_i - t_i)^2}{s}\right)^{\frac{1}{2}} \tag{10}$$

$$NRMSE = \left(\frac{\sum_{i=1}^{s}(E_i)^2}{s}\right)^{\frac{1}{2}} \tag{11}$$

$$MAE = \frac{\sum_{i=1}^{s}|p_i - t_i|}{s} \tag{12}$$

$$MARE = \frac{\sum_{i=1}^{s}\frac{|p_i - t_i|}{|t_i|}}{s} \tag{13}$$

$$CoC = \frac{s(\sum_{i=1}^{s} t_i p_i) - (\sum_{i=1}^{s} t_i)(\sum_{i=1}^{s} p_i)}{\sqrt{\left[s(\sum_{i=1}^{s} {p_i}^2) - (\sum_{i=1}^{s} p_i)^2\right]\left[s(\sum_{i=1}^{s} {t_i}^2) - (\sum_{i=1}^{s} t_i)^2\right]}} \quad (14)$$

$$CoD = CoC^2 \cong 1 - \frac{\sum_{i=1}^{s}(t_i - p_i)^2}{\sum_{i=1}^{s}(t_i - \tilde{t})^2} \quad (15)$$

$$CoE = \frac{\sum_{i=1}^{s}(t_i - \tilde{t})^2 - \sum_{i=1}^{s}(p_i - t_i)^2}{\sum_{i=1}^{s}(t_i - \tilde{t})^2} \quad (16)$$

$$MaxAE = MAX_{i=1}^{s}(|p_i - t_i|) \quad (17)$$

$$MaxARE = MAX_{i=1}^{s}\left(\frac{|p_i - t_i|}{|t_i|}\right) \quad (18)$$

where $\tilde{t}$ is the mean of the target values and:

$$E_i = \frac{p_i - t_i}{std(t)} \quad (19)$$

where $std(t)$ is the standard deviation of the target values.

5. Results and discussions

In this section, the main significant results are reported. In Figure 5 are reported the metrics values obtained, used to evaluate the fitness of the predicted PPs. In each bar graph (one for each adopted metric), is compared the related metric obtained for each PP. Prediction performances are very excellent for each of the eight predicted PPs. This is confirmed by the CoC, CoD, and CoE values which all approach 1. More in detail, the lower values are the CoD and CoE of fc (CF), which are equal to 0.9975. All the other used metrics underline as fc (CF) is the worst predicted variable. Metrics values for this PP prediction are otherwise acceptable, considering for example the MARE which is equal to 0.0019, with a MaxARE of 0.0171. The second worse predicted PP is the ηc (CF), which shows a MARE of 0.016 and a MaxARE of 0.0168. This confirms that the compressor health status prediction leads to lower performance. Also, note the marked difference between the value of the PPs related to the compressor and all the others. The better prediction performance instead is shown by the prediction of $\eta_{b,p}$. This parameter, related to the burner, shows a MARE of 0.00036, accompanied by a MaxARE of 0.003. CoC, CoD, and CoE metrics for ηb,p are all equal to 1. Figures 6-9 show the comparison between the predicted and the target values, and the percentage error of each observation, of the PPs related to the compressor, burner, spools, and electric motor and battery respectively. The percentage error reported in the just cited figures has been computed with the following equation:

$$E_{\%,i} = \frac{p_i - t_i}{t_i} 100 \quad (20)$$

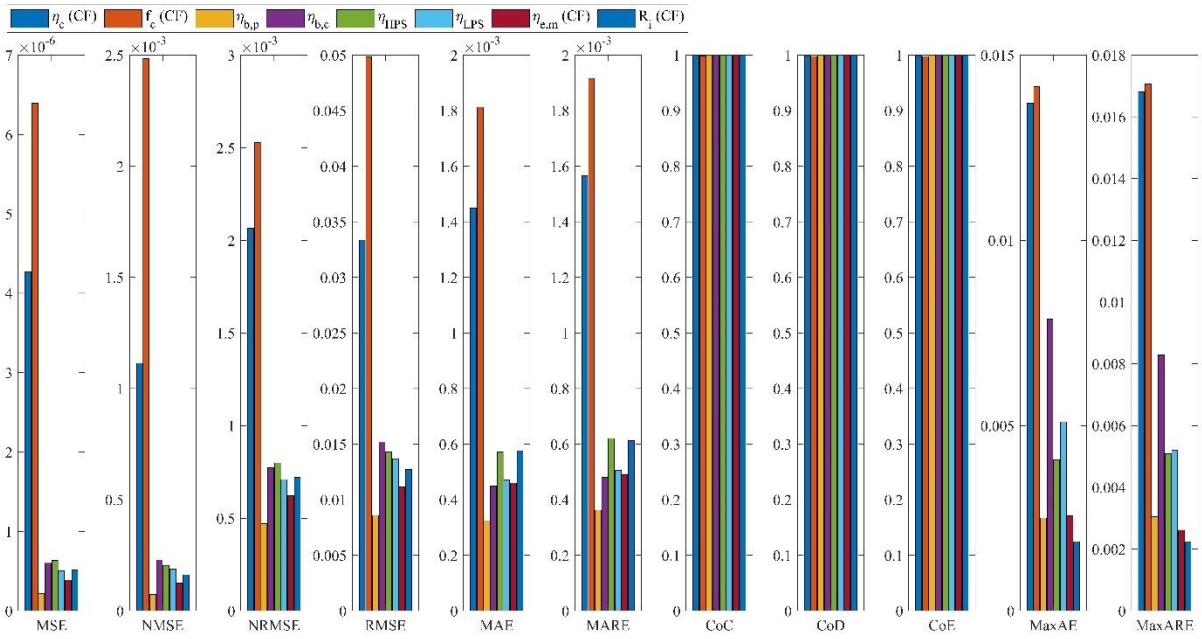

Figure 5. Metrics related to the prediction of the eight selected PPs.

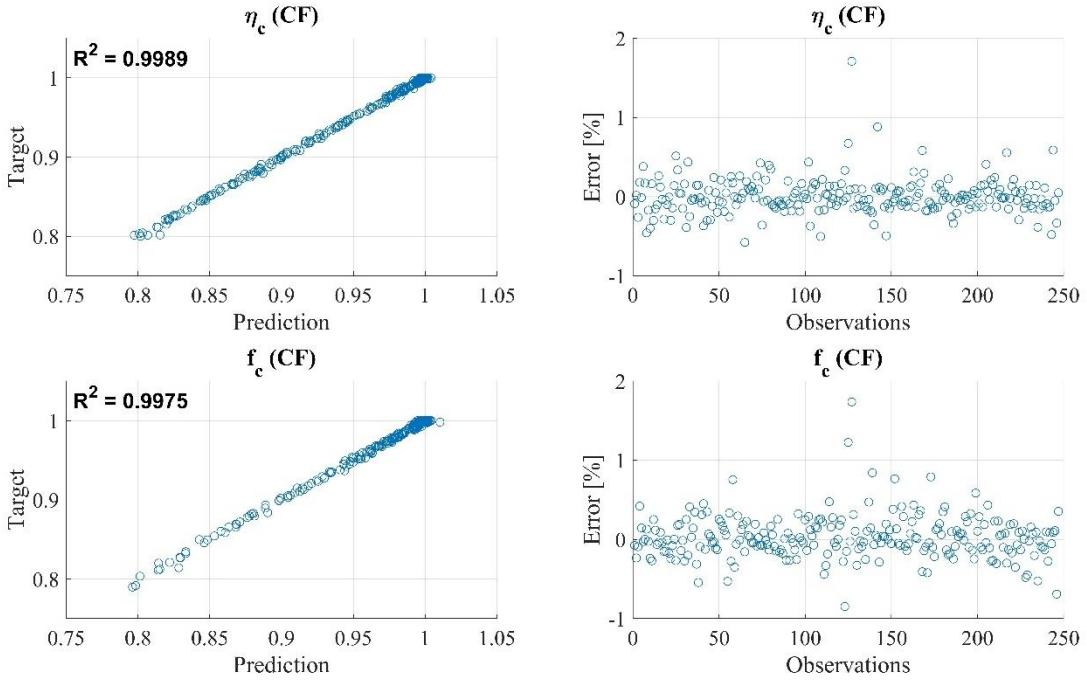

Figure 6. Comparison between prediction and target of the PPs related to the compressor.

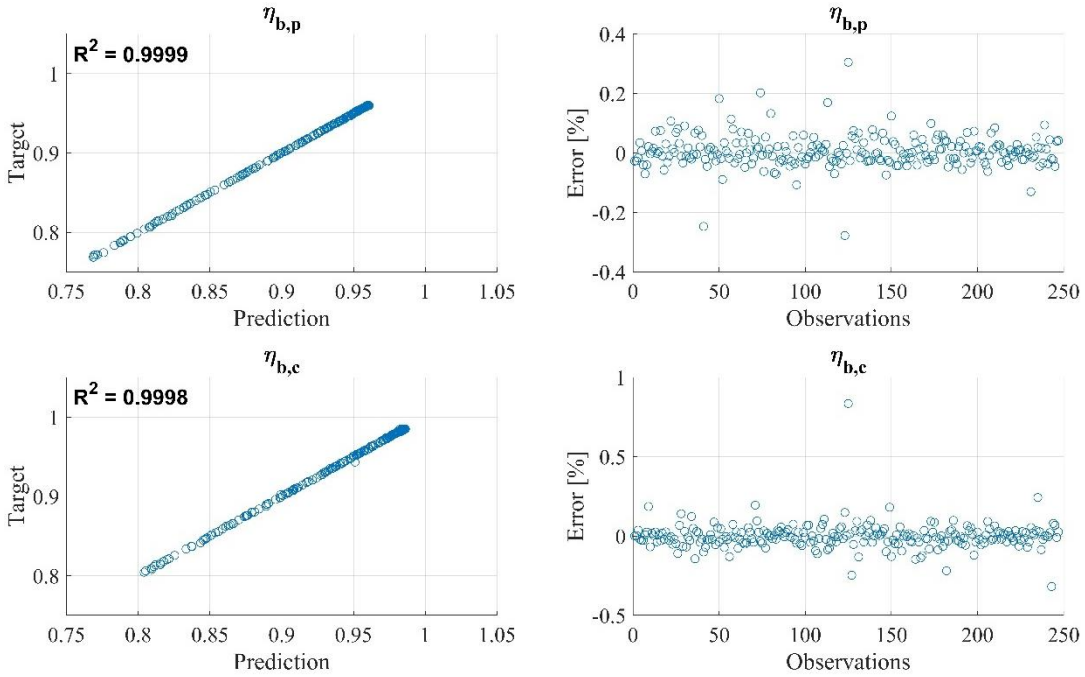

Figure 7. Comparison between prediction and target of the PPs related to the burner.

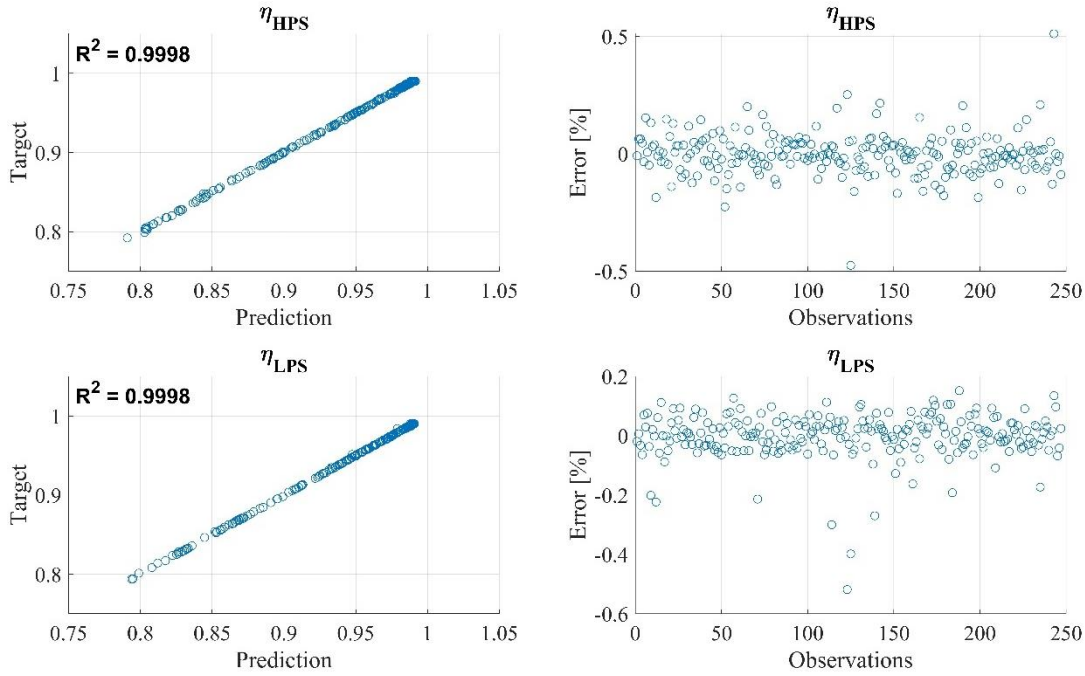

Figure 8. Comparison between prediction and target of the PPs related to the spools.

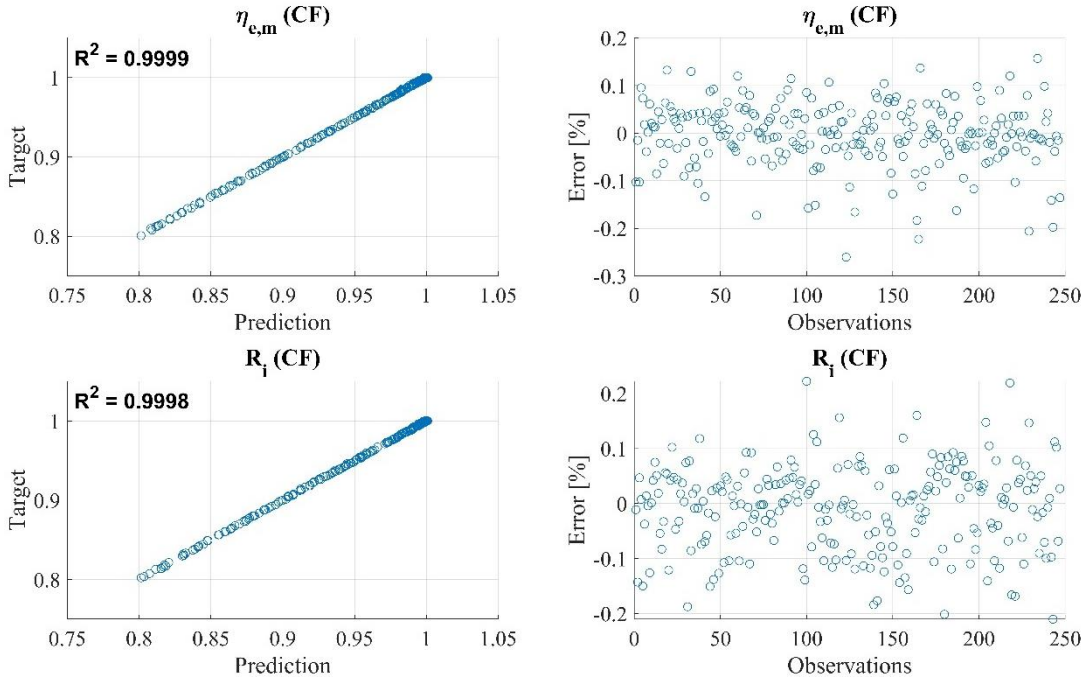

Figure 9. Comparison between prediction and target of the PPs related to the electric motor ($\eta_{e,m}$ (CF)) and battery (R_i (CF)).

Figure 6 confirms the slightly worse results obtained in the prediction of the PPs related to the compressor. Percentage errors instead are the highest, compared with the percentage errors of the other PPs. For ηc (CF) and fc (CF) prediction instead, almost all the observations have a percentage error below 1%, in absolute value. Figure 7 reports the same information for the prediction of the PPs related to the burner. In this case, the results are better, instead, almost all of the observations have a percentage error below 0.2%, in absolute value. The same result is true for the prediction of the PPs related to the spools and to the electric machine and the battery, as visible in Figures 8 and 9 respectively. Finally, the good performance obtained is further confirmed by the good correlation between target and predictions.

6. Conclusions

The present paper aimed to develop an efficient EHM system for PPs prediction in a hybrid turboshaft engine. The engine analyzed in this work was modeled using Simulink software. Subsequently, the Simulink model was exploited to perform a series of steady-state simulations in each of the four working points. In each simulation, a simultaneous degraded state of some selected components was implemented. The chosen components are the compressor, the burner, and the mechanical transmission of the spools for the thermal portion of the engine and the electric motor and the battery for the electric portion of the engine. The degraded state was implemented by applying a percentage variation with respect to the healthy condition to some PPs associated to the health status of the components. In particular, the selected PPs are the isentropic efficiency and flow parameter for compressor, pneumatic and combustion efficiencies for the burner, mechanical efficiency for spools, efficiency for the electric motor, and internal resistance for the battery. The value of the percentage variation of the PPs is different at each simulation and was randomly obtained. The results obtained from the simulations were used to obtain a dataset useful for the training and the resting processes of a FFNN, which was used in this paper as a tool for the prediction of the PPs. The results obtained from the application of the developed system for the prediction of the eight PPs were evaluated with the use of several error metrics, defined in section 4. The metrics obtained, shown in section 5, underline the very high performance of the developed system. Results are presented also with correlation and percentage error graphs. It is evident that all the

predictions have a relevant accuracy, with a slight worst performance in the prediction of the PPs related to the compressor. In particular, fc prediction shows the lower values of CoD and CoE, both equal to 0.9975, and the highest percentage errors, almost all below 1%, in absolute value. An efficient EHM tool is a very useful help to increase flight safety and decrease maintenance costs. A similar approach for a hybrid engine is still little researched in literature today. This paper aims to contribute to the enrichment of the information available.

References

[1] Singh S, Jain S, Venkateswaran P S, Tiwari A K, Nouni M R, Pandey J K, and Goel S 2015 Hydrogen: A sustainable fuel for future of the transport sector *Renew. Sust. Energ. Rev.* **51** 623–33 DOI: 10.1016/j.rser.2015.06.040.

[2] Yilmaz N and Atmanli A 2017 Sustainable alternative fuels in aviation *Energy* **140** 1378–86 DOI: 10.1016/j.energy.2017.07.077.

[3] Atilhan S, Park S, El-Halwagi M M, Atilhan M, Moore M and Nielsen R B 2021 Green hydrogen as an alternative fuel for the shipping industry. Curr. Opin. Chem. Eng. **31** 100668 DOI: 10.1016/j.coche.2020.100668.

[4] Masiol M and Harrison R M 2014 Aircraft engine exhaust emissions and other airport-related contributions to ambient air pollution: A review Atmos. Environ. **95** 409–55 DOI: 10.1016/j.atmosenv.2014.05.070.

[5] Adolfo D, Bertini D, Gamannossi A and Carcasci C 2017 Thermodynamic Analysis of an Aircraft Engine to estimate performance and emissions at LTO cycle Energy Procedia **126** 915–22 DOI: 10.1016/j.egypro.2017.08.162.

[6] Yildirim M T and Kurt B 2018 Aircraft Gas Turbine Engine Health Monitoring System by Real Flight Data. *Int. J. of Aero. Eng*. DOI: 10.1155/2018/9570873.

[7] Powrie H E G and Fisher C E 1999 Engine health monitoring: Towards total prognostics *1999 IEEE Aerospace Conference. Proceedings (Cat. No.99TH8403)* 07 March 1999 Snowmass, CO, USA 11–20 DOI: 10.1109/AERO.1999.789759.

[8] Meher-Homji C B, Chaker M and Bromley A F 2009 The Fouling of Axial Flow Compressors: Causes, Effects, Susceptibility, and Sensitivity *ASME Turbo Expo 2009: Power for Land, Sea, and Air* June 8–12 2009 Orlando, Florida, USA 571–90 DOI: 10.1115/GT2009-59239.

[9] Igie U, Goiricelaya M, Nalianda D and Minervino O 2016 Aero engine compressor fouling effects for short- and long-haul missions *Proc Inst Mech Eng G J Aerosp Eng* **230** 1312-24 DOI: 10.1177/0954410015607897.

[10] Fentaye A D, Baheta A T, Gilani S I and Kyprianidis K G 2019 A Review on Gas Turbine Gas-Path Diagnostics: State-of-the-Art Methods, Challenges and Opportunities. *Aerospace* **6** 83 DOI: 10.3390/aerospace6070083.

[11] Rezvanizaniani S M, Liu Z, Chen Y and Lee J 2014 Review and recent advances in battery health monitoring and prognostics technologies for electric vehicle (EV) safety and mobility. *J. Power Sources* **256** 110–24 DOI: 10.1016/j.jpowsour.2014.01.085.

[12] Donateo T, Ficarella A 2020 A Modeling Approach for the Effect of Battery Aging on the Performance of a Hybrid Electric Rotorcraft for Urban Air-Mobility. *Aerospace* **7** 56 DOI: 10.3390/aerospace7050056.

[13] DeRemer J E 1950 Sand and Dust Erosion in Aircraft Gas Turbines. *J. Am. Soc. Nav. Eng.* **62** 505–11.

[14] De Giorgi M G, Campilongo S, Ficarella A 2015 Predictions of Operational Degradation of the Fan Stage of an Aircraft Engine Due to Particulate Ingestion. *J Eng Gas Turbine Power* **137** DOI: 10.1115/1.4028769.

[15] Sripad S, Bills A, Viswanathan V 2021 A review of safety considerations for batteries in aircraft with electric propulsion *MRS Bull.* **46** 435–42 DOI: 10.1557/s43577-021-00097-1.

[16] De Giorgi M G, Ficarella A, De Carlo L 2019 Jet engine degradation prognostic using artificial neural networks. *Aircr. Eng. Aerosp. Technol.* **92** 296–303 DOI: 10.1108/AEAT-01-2018-0054.
[17] De Giorgi M G, Campilongo S, Ficarella A 2018 A diagnostics tool for aero-engines health monitoring using machine learning technique. *Energy Procedia* **148** 860–67 DOI: 10.1016/j.egypro.2018.08.109.
[18] De Giorgi M G, Campilongo S, Ficarella A 2018 Development of a real time intelligent health monitoring platform for aero-engine. *MATEC Web Conf* **233** 00007 DOI: 10.1051/matecconf/201823300007.
[19] Yildirim M T, Kurt B 2016 Engine health monitoring in an aircraft by using Levenberg-Marquardt Feedforward Neural Network and Radial Basis Function Network. *2016 International Symposium on INnovations in Intelligent SysTems and Applications (INISTA)* 02-05 August 2016 Sinaia, Romania 1–5 DOI: 10.1109/INISTA.2016.7571847.
[20] Donateo T, Terragno A and Ficarella A 2021 An optimized fuzzy logic for the energy management of a hybrid electric air-taxi *76th Italian National Congress* ATI September 2021 Rome
[21] Donateo T, De Pascalis C, Strafella L and Ficarella A 2021 Off-line and On-line Optimization of the Energy Management Strategy in a Hybrid Electric Helicopter for Urban Air-Mobility *Aerospace Science and Technology* **113**
[22] Donateo T, Cucciniello L, Strafella L and Ficarella A 2020 Control Oriented Modelling of a Turboshaft Engine for Hybrid Electric Urban Air-Mobility *E3S Web Conf* **197** 05003 DOI: 10.1051/e3sconf/202019705003.
[23] Mapped motor and drive electronics operating in torque-control mode - Simulink - MathWorks Italia, https://it.mathworks.com/help/autoblks/ref/mappedmotor.html (accessed 4 July 2022).
[24] Guzzella L and Sciarretta A 2013 *Vehicle Propulsion Systems* Springer.
[25] Hausmann A, Depcik C 2013 Expanding the Peukert equation for battery capacity modeling through inclusion of a temperature dependency *J. Power Sources* **235** 148–58 DOI: 10.1016/j.jpowsour.2013.01.174.
[26] Donateo T, De Pascalis C, Strafella L and Ficarella A 2021 Optimal Energy Management of a Hybrid Electric Helicopter for Urban Air-Mobility. *IOP Conf. Ser.: Mater. Sci. and Eng.* **1024** 012074.
[27] Taki M, Rohani A, Soheili-Fard F and Abdeshahi A 2017 Assessment of energy consumption and modeling of output energy for wheat production by neural network (MLP and RBF) and Gaussian process regression (GPR) models. *J. Clean. Prod.* **172** DOI: 10.1016/j.jclepro.2017.11.107.
[28] Botchkarev A 2019 Performance Metrics (Error Measures) in Machine Learning Regression, Forecasting and Prognostics: Properties and Typology. *arXiv preprint arXiv* **14** 045–076 DOI: 10.48550/arXiv.1809.03006

Acknowledgments
This research was funded by the Italian Ministry of University and Research, project PON “SMEA”, code PON03PE_00067_5